J. Fluid Mech. (2007), *vol.* 589, *pp.* 103–123. © 2007 Cambridge University Press
doi:10.1017/S0022112007007513 Printed in the United Kingdom

Velocity and temperature derivatives in high-Reynolds-number turbulent flows in the atmospheric surface layer. Part 3. Temperature and joint statistics of temperature and velocity derivatives

G. GULITSKI[1], M. KHOLMYANSKY[1], W. KINZELBACH[2], B. LÜTHI[2], A. TSINOBER[1] AND S. YORISH[1]

[1]Faculty of Engineering, Tel Aviv University, Tel Aviv 69978, Israel
[2]Institute of Environmental Engineering, ETH Zürich, CH-8093 Zürich, Switzerland

(Received 11 January 2006 and in revised form 19 May 2007)

This is part 3 of our work describing experiments in which explicit information was obtained on all the derivatives, i.e. spatial derivatives, $\partial/\partial x_j$, and temporal derivatives, $\partial/\partial t$, of velocity and temperature fields (and all the components of velocity fluctuations and temperature) at the Reynolds number $Re_\lambda \sim 10^4$.

This part is devoted to the issues concerning temperature with the emphasis on joint statistics of temperature and velocity derivatives, based on preliminary results from a jet facility and the main results from a field experiment. Apart from a number of conventional results, these contain a variety of results concerning production of temperature gradients, such as role of vorticity and strain, eigen-contributions, geometrical statistics such as alignments of the temperature gradient and the eigenframe of the rate-of-strain tensor, tilting of the temperature gradient, comparison of the true production of the temperature gradient with its surrogate. Among the specific results of importance is the essential difference in the behaviour of the production of temperature gradients in regions dominated by vorticity and strain. Namely, the production of temperature gradients is much more intensive in regions dominated by strain, whereas production of temperature gradients is practically independent of the magnitude of vorticity. In contrast, vorticity and strain are contributing equally to the tilting of the vector of temperature gradients.

The production of temperature gradients is mainly due to the fluctuative strain, the terms associated with mean fields are unimportant. It was checked directly (by looking at corresponding eigen-contributions and alignments), that the production of the temperature gradients is due to predominant compressing of fluid elements rather than stretching, which is true of other processes in turbulent flows, e.g. turbulent energy production in shear flows. Though the production of the temperature gradient and its surrogate possess similar univariate PDFs (which indicates the tendency to isotropy in small scales by this particular criterion), their joint PDF is not close to a bisector. This means that the true production of the temperature gradient is far from being fully represented by its surrogate. The main technical achievement is demonstrating the possibility of obtaining experimentally joint statistics of velocity and temperature gradients.

1. Introduction and motivation

There is an increasing interest in the behaviour of passive scalars in turbulent flows, as reflected in the large number of publications on various aspects of the issue, that have been reviewed in Majda & Kramer (1999), Shraiman & Siggia (2000), Warhaft (2000), Dimotakis (2001), Falkovich, Gawedzki & Vergassola (2001), Villermaux (2001) and Brethouwer, Hunt & Nieuwstadt (2003). The need to understand and predict micro-mixing in a variety of flows has promoted a number of studies devoted to the small-scale structure of scalar fields including the gradient, $\boldsymbol{G} = \nabla\theta$, of the scalar, θ. For example, better understanding of micro-mixing is vital for improving scalar molecular mixing models in turbulent flows, such as in the case of reactive fluids, since the mixing process controls the required fluxes of heat or chemical species to the reaction zone. Another example concerns stochastic Lagrangian models for the scalar fluctuations in a plume and their probability density functions (Sawford 2001). These stochastic models, however, depend on unproved concepts about micro-mixing mechanisms.

Just as velocity derivatives (both vorticity and strain) play an outstanding role in the dynamics of turbulence, the gradient, $\boldsymbol{G}$, is of the utmost importance in the evolution of the field of the passive scalar. Most common questions asked are about the statistical characteristics of the scalar itself (such as PDFs and structure functions/spectra) and (an)isotropy. All these are the consequence of the action of the turbulent flow on the passive scalar, which are reflected in joint statistical properties of the passive scalar and velocity fields. In the context of small-scale (dissipative) structure(s), these joint statistical properties relate to the derivatives of the corresponding fields. The experimental results for the two-point correlation, $\langle(\partial u_1/\partial x_1)_t(\partial\theta/\partial x_1)^2_{t+\tau}\rangle/\langle(\partial u_1/\partial x_1)^2\rangle^{1/2}\langle(\partial\theta/\partial x_1)^2\rangle$, indicate that the field of velocity derivatives produces scalar gradients on scales of about two Kolmogorov scales, i.e. on very small scales (Gibson, Ashurst & Kerstein 1988). Numerical simulations, as reviewed by Tsinober (2001), Vedula, Yeung & Fox (2001) and Brethouwer *et al.* (2003), give considerable attention to this last aspect.

The central issue here is the (one-way) interaction of the passive scalar gradient, $\boldsymbol{G}$, with the field of velocity derivatives, $\partial u_k/\partial x_i$, as seen from the equation (which is just the consequence of the advection-diffusion equation, $\partial\theta/\partial t + u_k(\partial\theta/\partial x_k) = \kappa\nabla^2\theta$), first given by Corrsin (1953) and Batchelor & Townsend (1956):

$$\frac{\mathrm{D}G_i}{\mathrm{D}t} = -G_k\frac{\partial u_k}{\partial x_i} + \kappa\nabla^2 G_i. \tag{1.1}$$

It is seen from this equation that the evolution of the gradient, $\boldsymbol{G}$, is subject to the effects of strain, rotation or tilting due to vorticity (accounted for by the term $-G_k\partial u_k/\partial x_i \equiv -G_j s_{ij} - (1/2)\varepsilon_{ijk}\omega_j G_k$) and molecular diffusion. The equation (1.1) governs both the dynamics of the magnitude of $\boldsymbol{G}$ and its direction.

We can obtain from (1.1) the corresponding 'energy' equation

$$\frac{1}{2}\frac{\mathrm{d}}{\mathrm{d}t}G^2 = -G_i G_k s_{ik} + G_i\kappa\nabla^2 G_i \tag{1.2}$$

and the equation for the unit vector, $\widehat{\boldsymbol{G}} = \boldsymbol{G}/G$:

$$\frac{\mathrm{d}}{\mathrm{d}t}\widehat{G}_i = \Upsilon_i + \mathrm{VT}, \tag{1.3}$$

where $\Upsilon_i = -\widehat{G}_k\partial u_k/\partial x_i + \widehat{G}_i\widehat{G}_j\widehat{G}_k s_{jk}$ and VT stands for viscous terms. The vector $\boldsymbol{\Upsilon}$ is orthogonal to $\boldsymbol{G}$.

One of the most important features of the small-scale evolution of passive scalars is their positive net production, $-\langle G_i G_k s_{ik}\rangle > 0$, and its rate, $-\langle G_i G_k s_{ik}/G^2\rangle > 0$. This was observed in numerical simulations in different flows (Ruetsch & Maxey 1991, 1992; Tsinober 2001; Tsinober & Galanti 2001; Vedula *et al.* 2001; Brethouwer *et al.* 2003 and references therein) at rather small Taylor microscale Reynolds numbers $Re_\lambda \sim 100$. No similar results have been obtained so far in the laboratory (with the exception of Su & Dahm (1996), who were able to obtain the alignments between the vector, $\boldsymbol{G}$, and the eigenframe, $\boldsymbol{\lambda}_k$, of the rate-of-strain tensor, s_{ij}, in the far field of a turbulent jet flow at $Re_\lambda \sim 50$), especially for high-Reynolds-number flows. Instead, a surrogate quantity, the mixed skewness,

$$S_\theta = \langle(\partial u_1/\partial x_1)(\partial\theta/\partial x_1)^2\rangle / \langle(\partial u_1/\partial x_1)^2\rangle^{1/2}\langle(\partial\theta/\partial x_1)^2\rangle, \tag{1.4}$$

was measured in several flows, as reviewed by Sreenivasan & Antonia (1997). For isotropic flows $\langle(\partial u_1/\partial x_1)(\partial\theta/\partial x_1)^2\rangle = (2/15)\langle G_i G_k s_{ik}\rangle$. However, surrogates of the type $(\partial u_1/\partial x_1)^m$, $(\partial\theta/\partial x_1)^n$ and $(\partial u_1/\partial x_1)^m(\partial\theta/\partial x_1)^n$ represent adequately only the means of the true quantities. Other properties (spectral, fractal, scaling, etc.) of the surrogates and of the true quantities are generally different.

By true quantities we mean quantities such as $G_i G_k s_{ik}$ which are geometrical invariants, i.e. they remain invariant under the full group of rotations in contrast to other non-invariant combinations of velocity and temperature derivatives. For this reason, the geometrical invariants are most appropriate for studying physical processes in turbulent flows, their structure and universal properties. Moreover, in using a single velocity or temperature difference or derivative, a number of important geometrical relations of extreme significance can be missed. For example, having single derivatives it is impossible to see the degree of alignment between the scalar gradient, G_i, and the stretching vector, $W_i^{G_s} \equiv -G_j s_{ij}$, which is at the core of the production of G^2, i.e. of the small-scale structure of passive scalars in turbulent flows. Similarly, having single derivatives, it is impossible to separate and study the effects of strain and of rotation or tilting of $\boldsymbol{G}$ due to vorticity, which influences the evolution of $\boldsymbol{G}$ in a qualitatively different manner, as far as is known from numerical simulations and simple models (Ruetsch & Maxey 1991, 1992; Tsinober & Galanti 2001, 2003; Gonzalez 2002; Brethouwer *et al.* 2003).

It was also realized from a number of numerical simulations (Ashurst *et al.* 1987; Ruetsch & Maxey 1991, 1992; Pumir 1994; Flohr 1999; Tsinober 2001; Tsinober & Galanti 2001, 2003; Vedula *et al.* 2001; Brethouwer *et al.* 2003) that the essential evolution of passive scalars, contained in the interaction between the scalar gradient, G_i, and the velocity gradients, $\partial u_k/\partial x_i$, depends strongly not only on the magnitude of $\boldsymbol{G}$, strain, s_{ij}, and vorticity, ω_i, but also on the joint geometry of the scalar gradient, G_i, and the field of velocity gradients, $\partial u_k/\partial x_i$. This is true of the magnitude of both $W_i^{G_s} \equiv -G_j s_{ij}$ and $W_i^{G_\omega} \equiv -(1/2)\varepsilon_{ijk}\omega_j G_k$ and the production term, $-G_i G_j s_{ij}$, which is just equal to the scalar product $\boldsymbol{G}\cdot\boldsymbol{W}^{G_s} \equiv -G_i G_j s_{ij} \equiv G W^{G_s}\cos(\boldsymbol{G}, \boldsymbol{W}^{G_s})$. It can be represented also as $-G_i G_j s_{ij} = -G^2 \Lambda_k \cos^2(\boldsymbol{G}, \boldsymbol{\lambda}_k)$ showing the importance of relative orientation of $\boldsymbol{G}$ and the eigenframe, $\boldsymbol{\lambda}_k$, of the rate-of-strain tensor, s_{ij}, and the relation between separate eigen-contributions, $-G^2\Lambda_\alpha \cos^2(\boldsymbol{G}, \boldsymbol{\lambda}_\alpha)$ (no summation over α); here Λ_α are the eigenvalues of s_{ij}.

The evolution of $\boldsymbol{G}$ in a turbulent flow is associated with creation of fine structure in the field of the passive scalar, both at the level of the gradient, G_i, itself and at the level of its gradients, $\partial G_i/\partial x_k$. The positiveness of the term $-\langle G_i G_k s_{ik}\rangle$ (and $-\langle G_i G_k s_{ik}/G^2\rangle$) is associated with two aspects. First, it represents the rate of production of the 'dissipation' $\kappa\langle G^2(t)\rangle$ of the 'energy' of the passive scalar, so that

the latter is continuously amplified by the stretching process reflected in the term $-\langle G_i G_k s_{ik}\rangle$. Production of the gradients, $G^2(t)$, of a scalar field is associated with the fine structure of the passive scalar, θ, itself. Secondly, the term $-\langle G_i G_k s_{ik}\rangle$ is balanced, at least in part, by the 'dissipation', $-\kappa\langle(\partial G_i/\partial x_k)(\partial G_i/\partial x_k)\rangle$, of the 'energy' of the vector $\boldsymbol{G}$. The consequence is that the gradients, $\partial G_i/\partial x_k$, associated with the fine structure of $\boldsymbol{G}$, are amplified too.

In concluding this section we reiterate that all the quantities mentioned above, such as $-G_k(\partial u_k/\partial x_i)$, $-\varepsilon_{ijk}\omega_j G_k/2$, $-G_i G_k s_{ik}$ and a number of others (see next section) are essentially mixed quantities, involving both the field of velocity derivatives (strain and vorticity) and the gradients of the scalar field. This reflects the obvious fact that the properties of a passive scalar field are determined by the (one-way) interaction of both fields. Hence, the importance of studying the joint statistical properties of both scalar gradient, $\partial\theta/\partial x_i$, and the velocity gradients, $\partial u_k/\partial x_i$.

2. Main objectives

The above overview comprises the basis for setting as the main goal of the work reported here the study of the joint statistical properties of the velocity derivatives and the gradient of the passive scalar. We stress that at high Reynolds numbers, except for the mixed skewness, nothing is known about the issues mentioned above and many other important issues. It should also be emphasized that these key issues cannot be addressed via conventional approaches using phenomenological, scaling and similar arguments, which inherently are unable to handle the geometrical (and phase) relations in turbulent flows.

More specifically, the first and main objective of the reported work is a systematic study of the joint statistical properties of the field of velocity derivatives, i.e. rate-of-strain tensor, s_{ij}, and vorticity, ω_i, and the temperature gradient, G_i, in an atmospheric surface layer at $Re_\lambda \sim 10^4$. It is done in a similar way to that in the field experiment on the ground of Kfar Glikson kibbutz, a few kilometres to the north-east of Pardes-Hanna, as described in Kholmyansky & Tsinober (2000) and Kholmyansky, Tsinober & Yorish (2001*a*, *b*) (see Part 1, Gulitski *et al.* 2007).

The main basis of the work is a new data set obtained for all three components of the velocity fluctuations vector, u_i, all nine components of the spatial velocity gradients tensor, $\partial u_i/\partial x_j$, and the temporal velocity derivatives, $\partial u_i/\partial t$ (all without invoking the Taylor hypothesis) with synchronous data on fluctuations of temperature, θ, its spatial gradient, $\partial\theta/\partial x_j$, and temporal derivative, $\partial\theta/\partial t$, along with the corresponding data on the mean flow. The subsequent post-processing and analysis were performed along several lines in order to achieve a deeper understanding of the basic properties and processes of the fine structure of the passive scalar. It is the availability of such data which allows us to address the issues which are essentially beyond phenomenology. Typical examples are represented by the following quantities.

(i) The stretching vector, $W_i^G \equiv -G_k\partial u_k/\partial x_i \equiv -G_j s_{ij} - (1/2)\varepsilon_{ijk}\omega_j G_k$, and its components, $W_i^{G_s} \equiv -G_j s_{ij}$ and $W_i^{G_\omega} \equiv -(1/2)\varepsilon_{ijk}\omega_j G_k$. The vector $W_i^{G_s}$ is responsible for the production of G^2, whereas $W_i^{G_\omega}$ (which is normal to $\boldsymbol{G}$) rotates/tilts the vector $\boldsymbol{G}$. Of interest also is the vector $\Upsilon_i = -\widehat{G}_k\partial u_k/\partial x_i + \widehat{G}_i\widehat{G}_j\widehat{G}_k s_{jk}$, which rotates the unit vector, $\widehat{G}_i = G_i/G$.

(ii) The production, $-G_i G_j s_{ij}$, and its rate, $-G_i G_j s_{ij}/G^2$.

(iii) The eigen-contributions to the production, $-G^2\Lambda_1\cos^2(\boldsymbol{G}, \boldsymbol{\lambda}_1)$, $-G^2\Lambda_2\cos^2(\boldsymbol{G}, \boldsymbol{\lambda}_2)$, $-G^2\Lambda_3\cos^2(\boldsymbol{G}, \boldsymbol{\lambda}_3)$, the rates, $-\Lambda_1\cos^2(\boldsymbol{G}, \boldsymbol{\lambda}_1)$, $-\Lambda_2\cos^2(\boldsymbol{G}, \boldsymbol{\lambda}_2)$,

$-\Lambda_3 \cos^2(\boldsymbol{G}, \boldsymbol{\lambda}_3)$, and the similar contributions to $(W^G)^2$, $(W^{G_s})^2$, $(W^{G_\omega})^2$ and the corresponding rates.

(iv) Geometrical statistics, associated with the above quantities, such as $\cos(\boldsymbol{G}, \boldsymbol{\omega})$, $\cos(\boldsymbol{G}, \boldsymbol{\lambda}_i)$, $\cos(\boldsymbol{G}, \boldsymbol{W}^{G_s})$, $\cos(\boldsymbol{G}, \boldsymbol{W}^{G_\omega})$ and $\cos(\boldsymbol{\Upsilon}, \boldsymbol{\lambda}_k)$.

Having all the derivatives of the velocity and temperature field enables us to address the issue of isotropy in a variety of ways. The simplest one, related to the joint statistics of both fields, is via the relation $\langle(\partial u_1/\partial x_1)(\partial\theta/\partial x_1)^2\rangle = (2/15)\langle G_i G_k s_{ik}\rangle$ which is valid for isotropic flow.

There is a claim that vorticity influences essentially the statistics of passive scalars (Gonzalez & Paranthoën 2004 and references therein), though there is no such evidence in other works (Brethouwer *et al.* 2003 and references therein). Finally, the issue of anisotropy in small scales is intimately related to the direct and bi-directional coupling of small and large scales (Shen & Warhaft 2000; Warhaft 2000; Tsinober 2001). We can cope with the latter issue looking at joint statistics of the derivatives and the quantities themselves (which are available too) in a similar way to that in Kholmyansky & Tsinober (2000) and references therein.

3. Preliminary results in a jet facility

The main purpose of these experiments was to check the feasibility of obtaining sensible results on joint statistics of the velocity derivatives and the gradient of a passive scalar.

The jet facility, based on the calibration unit, was described briefly in Part 1. The jet was produced by a nozzle with outlet diameter $D = 30\,\mathrm{mm}$, the flow velocity at the outlet was about $10\,\mathrm{m\,s^{-1}}$. The measurement point was at the distance $4.3D \sim 13\,\mathrm{cm}$ from the nozzle.

The first example is shown in figure 1. As in many other cases, there are three main outcomes. First, the possibility of obtaining such statistics is demonstrated. Secondly, the results appear to be qualitatively the same as those obtained at much smaller Reynolds numbers $Re_\lambda \sim 100$ in DNS in a cubic domain with periodic boundary conditions and large-scale forcing $F_T = C(\sin x + \sin y + \sin z)$ on the right-hand side of the Navier–Stokes equations (Tsinober & Galanti 2001). Thirdly, there exists an essential difference in the behaviour of the production of temperature gradients in regions dominated by vorticity and strain. Namely, the production of temperature gradients is much more intensive in regions dominated by strain, whereas it is practically independent of the magnitude of vorticity. The results shown in figure 1 appear to be of a universal nature, at least qualitatively, as can be seen from comparison between the results at $Re_\lambda \sim 100$ from DNS in a cubic domain, the experimental results at $Re_\lambda \sim 800$ in a jet flow and, as shown below, in a field experiment in the atmospheric surface layer at several heights at Re_λ up to 8000 (see figure 7).

The next example is on geometrical statistics, see figure 2 which shows the alignments between the temperature gradient, $\boldsymbol{G}$, and the eigenframe, $\boldsymbol{\lambda}_i$, of the rate-of-strain tensor, s_{ij}. Again it is seen that, at least at the qualitative level, the results from experiments and DNS are the same (and they are the same for the field experiments as well, see figure 19). The main effect, the alignment between the temperature gradient and the eigenvector, $\boldsymbol{\lambda}_3$, corresponding to the compressive eigenvalue, $\Lambda_3 < 0$, is captured well in the measurements and is again similar to that obtained from DNS. Weaker alignment in the experiments is most probably due to some under-resolution of the velocity and temperature gradients. This kind of alignment was observed also

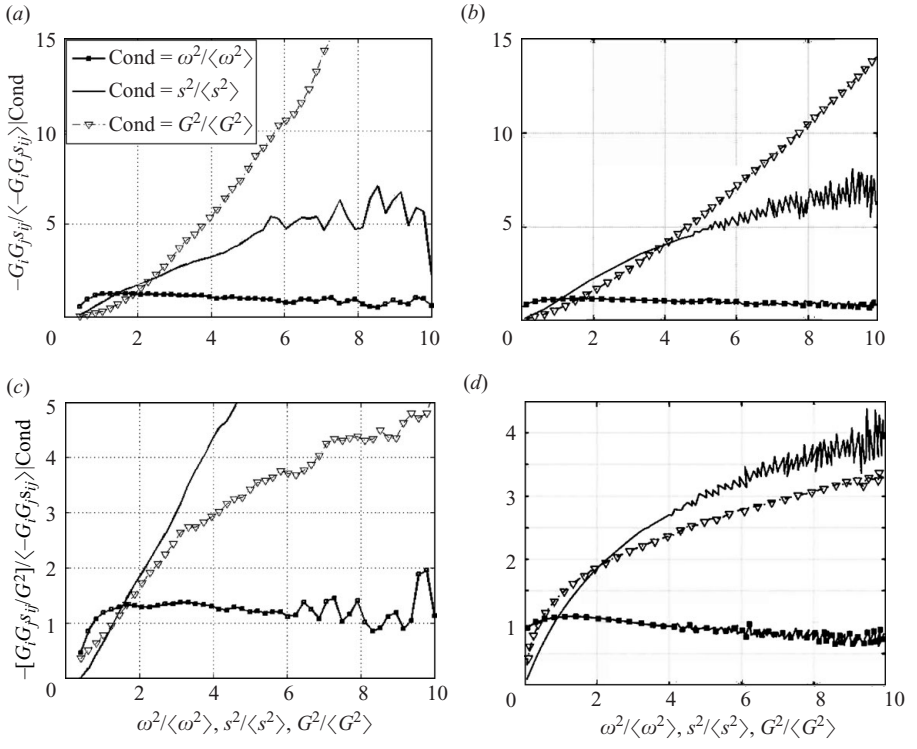

FIGURE 1. (*a*, *b*) Conditional averages of the normalized production of temperature fluctuations, $-G_iG_ks_{ik}$, and (*c*, *d*) its rate, $-G_iG_ks_{ik}/G^2$, conditioned on ω^2, s^2 and G^2. (*a*, *c*) Experiment with a heated jet; (*b*, *d*) direct numerical simulation of Navier–Stokes equations.

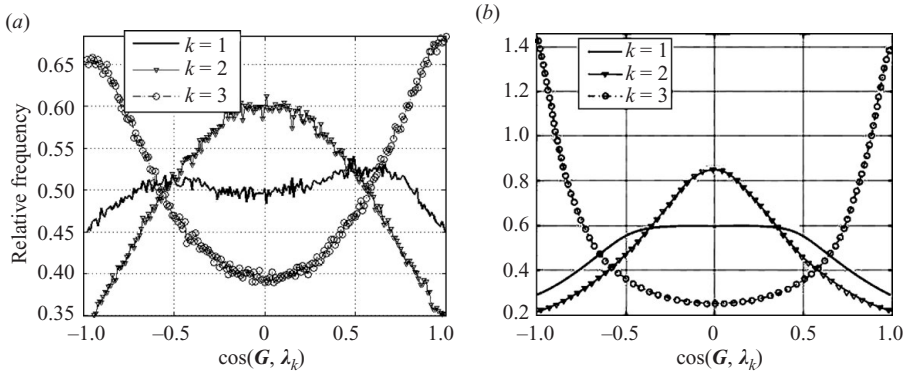

FIGURE 2. PDFs of the cosine of the angle between the temperature gradient, $\boldsymbol{G}$, and the eigenframe, $\boldsymbol{\lambda}_i$, of the rate-of-strain tensor, s_{ij}. (*a*) The experiment with a heated jet; (*b*) direct numerical simulation of Navier–Stokes equations.

in experiments by Su & Dahm (1996) and in DNS by Flohr (1999) and Tsinober & Galanti (2001, 2003).

Finally, the third example shows that the alignment between the temperature gradient and the eigenvector, $\boldsymbol{\lambda}_3$, corresponding to the compressive eigenvalue, is associated with the main contribution to the production term, $-G_iG_js_{ij} = -G^2\Lambda_k\cos^2(\boldsymbol{G}, \boldsymbol{\lambda}_k)$,

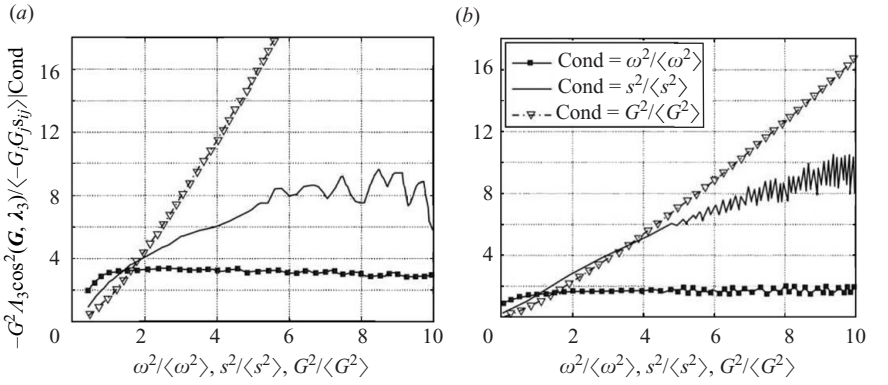

FIGURE 3. Conditional averages of the normalized contribution of the term, associated with the eigenvector, $\boldsymbol{\lambda}_3$, of the rate-of-strain tensor, s_{ij}, to the production of temperature fluctuations, conditioned on ω^2, s^2 and G^2. (*a*) The experiment with a heated jet; (*b*) direct numerical simulation of Navier–Stokes equations.

and the rate of production, $-G_iG_js_{ij}/G^2 = -\Lambda_k\cos^2(\boldsymbol{G}, \boldsymbol{\lambda}_k)$, namely, it is due to $-G^2\Lambda_3\cos^2(\boldsymbol{G}, \boldsymbol{\lambda}_3)$ (figure 3). Again, the similarity between the results from laboratory experiments and DNS can be seen clearly. We will see below that this similarity is much broader and remains valid also for the field experiments at much larger Reynolds numbers.

The production of the temperature gradient is due to the predominant compression of fluid elements rather than stretching.

4. Results of field experiments

As mentioned, our main purpose was to study the quantities associated with the production of gradient, $\boldsymbol{G}$, of the passive scalar. The quantity responsible for this process is the stretching vector, $W_i^G \equiv -G_k\partial u_k/\partial x_i \equiv -G_js_{ij} - (1/2)\varepsilon_{ijk}G_j\omega_k$. One of the key quantities is the term $-G_iG_js_{ij}$ in (1.2) associated with the production of the magnitude, G, of the temperature gradient, $\boldsymbol{G}$. Another quantity is the one responsible for the change in the direction of $\boldsymbol{G}$. This is the tilting vector, $\Upsilon_i = -\widehat{G}_k(\partial u_k/\partial x_i) + \widehat{G}_i\widehat{G}_j\widehat{G}_ks_{jk}$ (see (1.4)) which rotates the unit vector, $\widehat{G}_i = G_i/G$. Both are related to non-diffusive effects associated with the field of velocity derivatives. The effects directly related to diffusivity (i.e. the Laplacian of $\boldsymbol{G}$, etc.) are beyond the scope of our work.

4.1. *Some general results*

4.1.1. *Temperature*

The measurements (Part 1) were performed at several heights above the ground from 0.8 to 10 m. The span of the mean temperature, T, was about 2 K. The mean temperature was measured independently, at six heights from 0.5 to 11.5 m. The vertical temperature profile, averaged over the duration of the presented runs (about 3 h), is shown in figure 4(*a*). (The temperature at the lowest height is most probably underestimated because of insufficient delay before reading the value after the return of the device from the top position.) The linear fit, also shown on the plot, is found to be $\log_{10}(z) = 15.703 - 1.318T$. The thermal stability at the site, when our measurements were performed, can be described as slight instability. The typical PDF

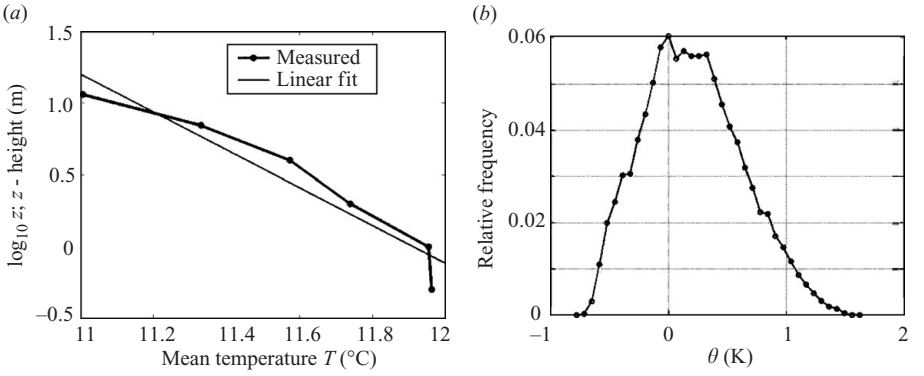

FIGURE 4. (*a*) Vertical temperature profile, averaged over the duration of the runs; (*b*) Example of PDF of the temperature fluctuations, θ.

Height (m)	0.8	1.2	2.0	3.0	4.5	7.0	10.0
θ RMS (K)	0.46	0.45	0.43	0.40	0.33	0.29	0.23

TABLE 1. The RMS values of θ for various heights.

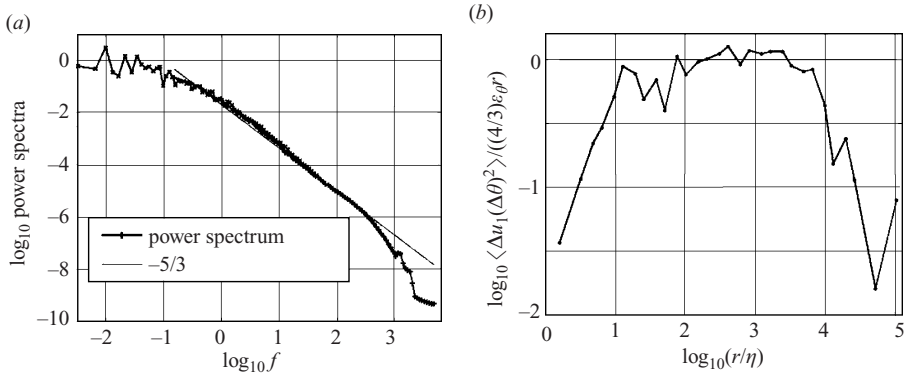

FIGURE 5. (*a*) Examples of the power spectrum of θ (for height 2 m) and (*b*) of the normalized mixed velocity–temperature structure function ($-4/3$ Yaglom law).

of the temperature fluctuations, θ, is presented in figure 4(*b*). The RMS values of θ for various heights are shown in table 1.

An example of the power spectrum of θ is plotted in figure 5(*a*) for the height of 2 m. In figure 5(*b*) we show an example of the normalized structure function, $-\langle \Delta u_1 (\Delta\theta)^2 \rangle (4\epsilon_\theta r/3)^{-1}$; $\Delta u_1 = u_1(x_1+r) - u_1(x_1)$; $\Delta\theta = \theta(x_1+r) - \theta(x_1)$; $\epsilon_\theta = \kappa \langle (\nabla\theta)^2 \rangle$ is the dissipation of the passive scalar variance; κ is the thermal diffusivity of air.

4.1.2. *RDT-like terms*

As in the case of velocity derivatives, our main interest here was in the field of derivatives of temperature fluctuations, $\partial\theta/\partial x_k$. However, in order to be able to limit ourselves to measurements of this field only, it was necessary to estimate the influence of the processes associated with the mean temperature and velocity gradients, $\partial T/\partial x_k \equiv \boldsymbol{\Theta}$ and $\partial U_i/\partial x_k$, on the production of $G_k \equiv \partial\theta/\partial x_k$.

Heigh (m)	0.8	1.2	2.0	3.0	4.5	7.0	10.0
Maximum ratio	0.0008	0.0008	0.0004	0.0004	0.0003	0.0005	0.0004

TABLE 2. Maximum absolute values of the ratio of the terms, associated with the mean flow gradient (4.1), to the main production term, $-\langle G_i G_k s_{ik}\rangle$.

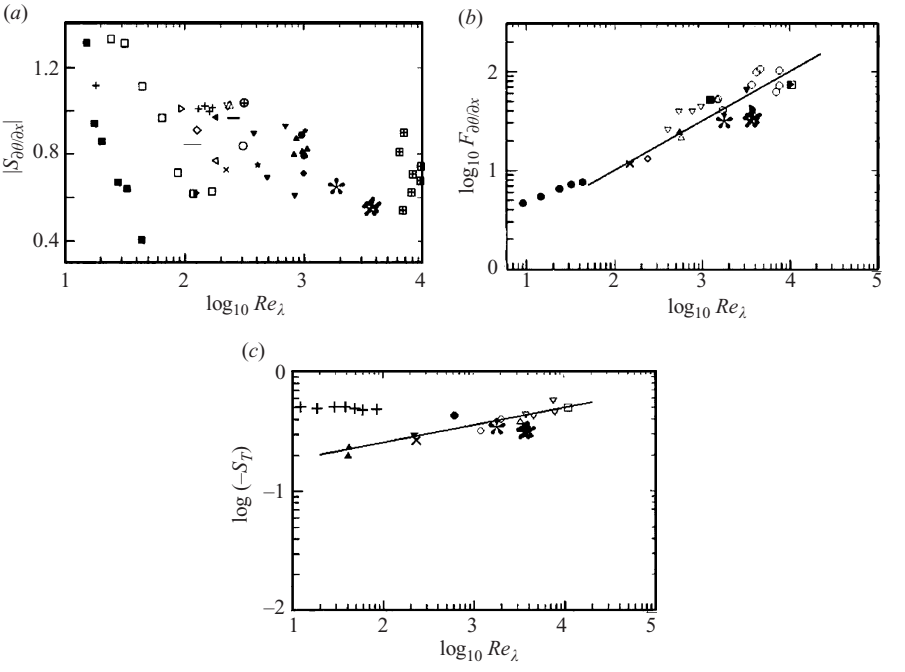

FIGURE 6. (*a*) Temperature derivative skewness, (*b*) flatness and (*c*) mixed derivative skewness, S_T, versus Reynolds number, Re_λ. Asterisks, present work, the explanation of other symbols see Sreenivasan & Antonia (1997).

There are three quantities of this kind in the equation for G^2:

$$-G_i s_{ik}\partial T/\partial x_k,\ -(1/2)\boldsymbol{G}\cdot(\boldsymbol{\Theta}\times\boldsymbol{\omega}) \equiv -(1/2)\boldsymbol{\Theta}\cdot(\boldsymbol{G}\times\boldsymbol{\omega}),\ -G_i G_k \partial U_i/\partial x_k. \qquad (4.1)$$

It is known from numerical simulations for moderate Reynolds numbers (Tsinober & Galanti 2001; Vedula *et al.* 2001) that the means $-\langle G_i s_{ik}\rangle\partial T/\partial x_k$, $-(1/2)\boldsymbol{\Theta}\cdot\langle\boldsymbol{G}\times\boldsymbol{\omega}\rangle$ and $-\langle G_i G_k\rangle\partial U_i/\partial x_k$ are small. We see from table 2 that in our experiments these quantities are small compared to the production term, $-\langle G_i G_k s_{ik}\rangle$.

4.2. *Skewness and flatness*

Most of the quantities derived from our experiments and reported here are of the order of two or less with respect to temperature. All our data are satisfactory for obtaining them. Higher-order moments, such as skewness and flatness, are much more sensitive to any flaws in the data. At 4.5 m and higher, the signal-to-noise ratio happened to be insufficient for good estimates of such moments. Other reasons led to the same effect at the lowest height of 0.8 m. Therefore in this section we present only the results, measured at 1.2, 2.0 and 3.0 m.

In figure 6, we reproduce the plots from (Sreenivasan & Antonia 1997, figures 7–9) with the addition of the points from the runs of our field experiment mentioned

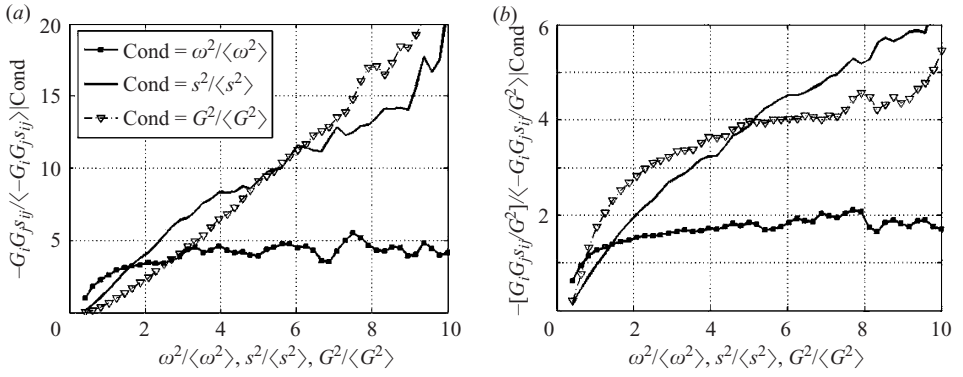

FIGURE 7. (*a*) Conditional averages of the normalized production of temperature fluctuations, $-G_iG_js_{ij}$, and (*b*) its rate, $-G_iG_js_{ij}/G^2$, conditioned on ω^2, s^2 and G^2. The field experiment.

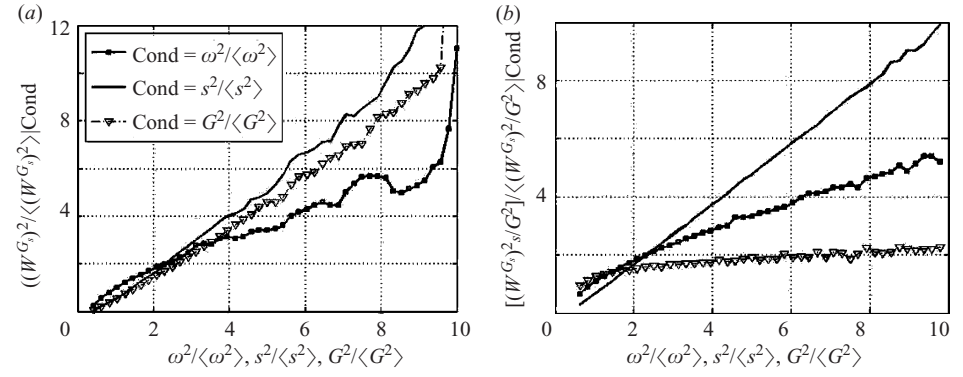

FIGURE 8. (*a*) Conditional averages of the normalized square of the stretching vector, $(W^{G_s})^2$, and (*b*) its rate, $(W^{G_s})^2/G^2$, conditioned on ω^2, s^2 and G^2.

above. In figure 6(*a*) the skewness of $\partial\theta/\partial x_1$, namely, $\langle(\partial\theta/\partial x_1)^3\rangle/\langle(\partial\theta/\partial x_1)^2\rangle^{3/2}$, is plotted versus the Reynolds number, Re_λ. Figure 6(*b*) shows the Re_λ-dependence of the derivative flatness, $\langle(\partial\theta/\partial x_1)^4\rangle/\langle(\partial\theta/\partial x_1)^2\rangle^2$. Finally, in figure 6(*c*) there is a plot of the mixed derivative skewness, $S_T \equiv \langle(\partial u_1/\partial x_1)(\partial\theta/\partial x_1)^2\rangle/\langle(\partial u_1/\partial x_1)^2\rangle^{1/2}\langle(\partial\theta/\partial x_1)^2\rangle$. Our points reasonably fit the results of other authors, presented in figure 6.

4.3. *Role of vorticity and strain*

The main result here is, as already mentioned in § 3, the same as at lower Reynolds numbers both in experiments and DNS. Namely, the production of temperature gradients is much more intensive in regions dominated by strain, whereas this production is practically independent of (or weakly dependent on) the magnitude of vorticity. This is true both of production, $-G_iG_js_{ij}$, and its rate, $-G_iG_js_{ij}/G^2$, (figure 7) as well as of the square of the stretching vector, $(W^{G_s})^2$, and its rate, $(W^{G_s})^2/G^2$ (figure 8). Thus in this respect, our results do not confirm the predictions of Gonzalez & Paranthoën (2004) and previous papers that vorticity influences essentially the statistics of passive scalars. However, as expected, the tilting of the gradient, $\boldsymbol{G}$, i.e. the change of its direction by $\Upsilon_i = -\widehat{G}_k(\partial u_k/\partial x_i) + \widehat{G}_i\widehat{G}_j\widehat{G}_k s_{jk}$ is equally influenced by strain and vorticity, as can be seen both from the conditional averages of Υ^2 on ω^2 and s^2 (figure 9) and the joint PDFs of Υ^2 with ω^2 and with

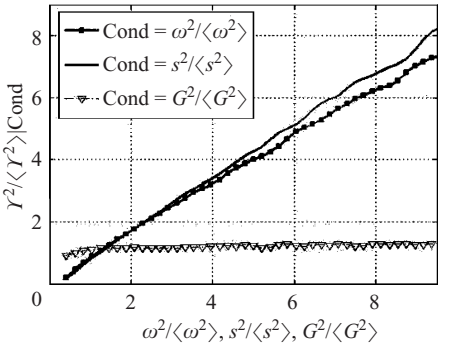

FIGURE 9. Conditional averages of the normalized square of the tilting vector, Υ^2, conditioned on ω^2, s^2 and G^2.

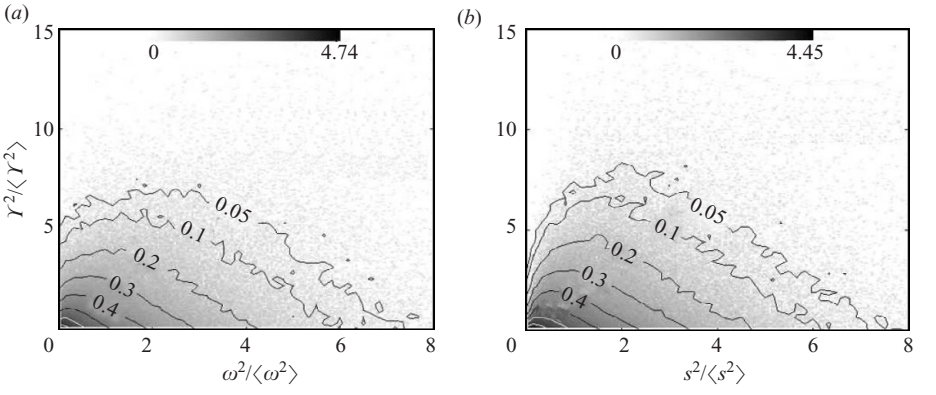

FIGURE 10. (*a*) Joint PDFs of the normalized square of the tilting vector, Υ^2, with normalized ω^2 and (*b*) s^2. Density shows $\log_{10}$ number of points. (*a*) Correlation coefficient = 0.528; (*b*) 0.504.

s^2 (figure 10). This is reminiscent of the influence of vorticity on the evolution of material elements, studied by Girimaji & Pope (1990) and Guala *et al.* (2005). The tilting is insensitive to the magnitude of $\boldsymbol{G}$, as seen from the figure 9.

A similar behaviour is observed when looking at separate eigen-contributions to the above quantities, and is described in the next section.

4.4. *Eigen-contributions*

By the expression 'eigen-contribution' we mean the separate terms in, for example, representation

$$-G_iG_js_{ij} = -G^2\Lambda_1\cos^2(\boldsymbol{G},\boldsymbol{\lambda}_1) - G^2\Lambda_2\cos^2(\boldsymbol{G},\boldsymbol{\lambda}_2) - G^2\Lambda_3\cos^2(\boldsymbol{G},\boldsymbol{\lambda}_3).$$

The first result we would like to show in this section concerns the relation of the eigen-contributions in the above representation with strain, vorticity and the magnitude of the temperature gradient. The corresponding conditional averages are presented in figure 11(*a*) and exhibit tendencies as described in the previous section, i.e. much stronger influence of strain than of vorticity.

This is true also of other quantities, e.g. $(W^{G_s})^2 = G^2\Lambda_k^2\cos^2(\boldsymbol{G},\boldsymbol{\lambda}_k)$, (figure 12*a*) and corresponding rates, $G_iG_js_{ij}/G^2 = \Lambda_k\cos^2(\boldsymbol{G},\boldsymbol{\lambda}_k)$ (figure 11*b*) and $(W^{G_s})^2/G^2 = \Lambda_k^2\cos^2(\boldsymbol{G},\boldsymbol{\lambda}_k)$ (figure 12*b*).

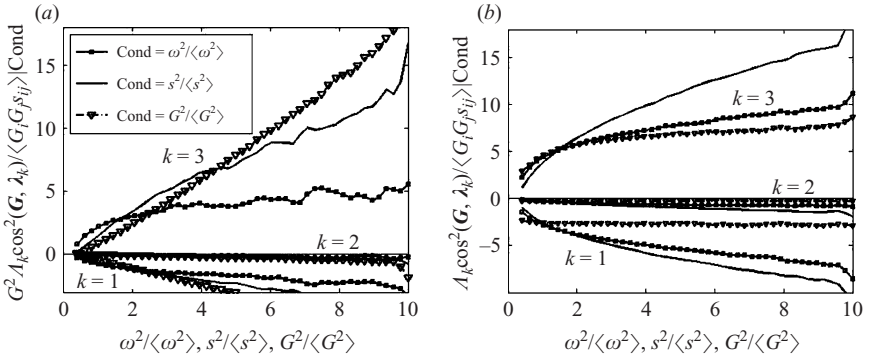

FIGURE 11. (*a*) Conditional averages of the eigen-contributions to the normalized production of temperature fluctuations, $-G_i G_j s_{ij}$, and (*b*) its rate, $-G_i G_j s_{ij}/G^2$, on ω^2, s^2 and G^2.

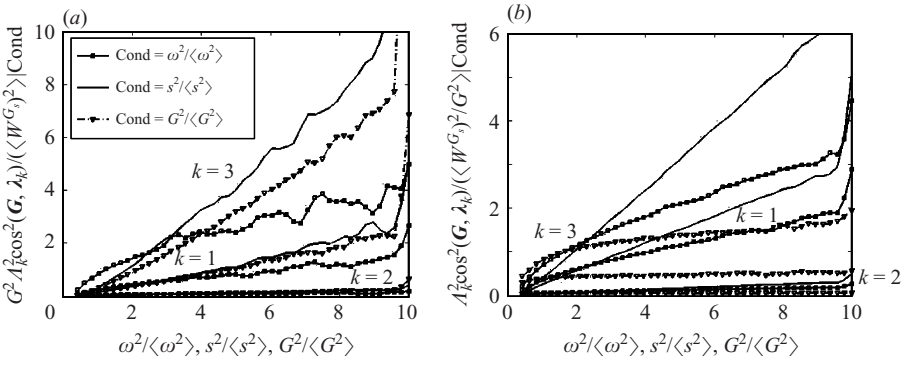

FIGURE 12. (*a*) Conditional averages of the eigen-contributions to the normalized square of the stretching vector, $(W^{G_s})^2$, and (*b*) its rate, $(W^{G_s})^2/G^2$, on ω^2, s^2 and G^2.

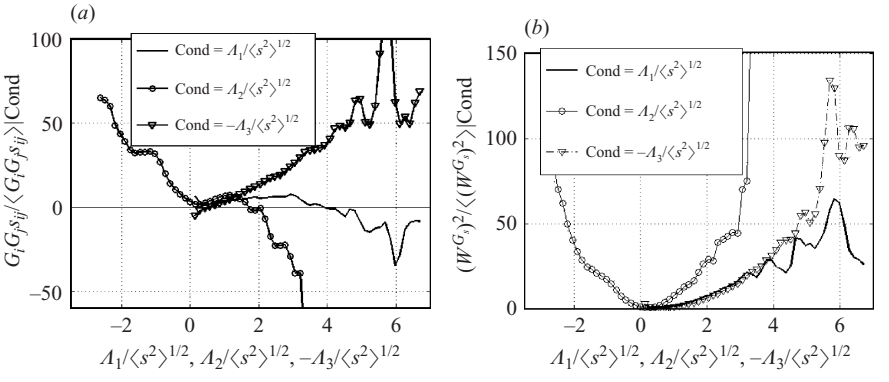

FIGURE 13. (*a*) Conditional averages of the normalized production of temperature fluctuations, $-G_i G_j s_{ij}$, and (*b*) of the normalized square of the stretching vector, $(W^{G_s})^2$, on the eigenvalues of the rate-of-strain tensor, Λ_k.

Useful information is contained also in the conditional averages of production of temperature fluctuations, $-G_i G_j s_{ij}$, and its rate, $-G_i G_j s_{ij}/G^2$, on the eigenvalues, Λ_k. The main feature is the dominance of the contribution associated with compression at large Λ_3 (figure 13).

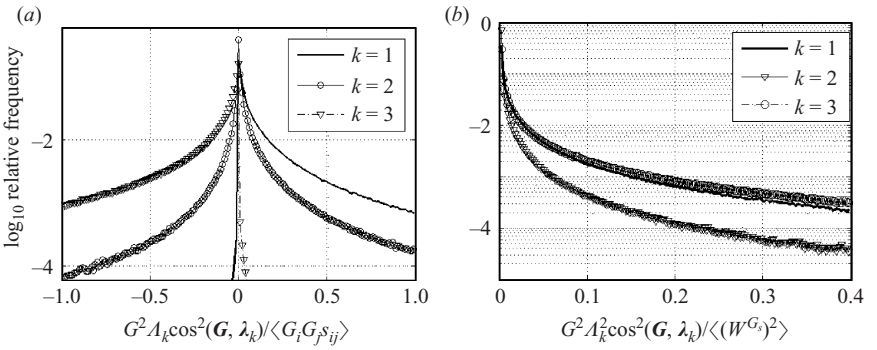

FIGURE 14. (*a*) PDFs of the eigen-contributions to the normalized production of temperature fluctuations, $-G_iG_js_{ij}$, and (*b*) the normalized square of the stretching vector, $(W^{G_s})^2$.

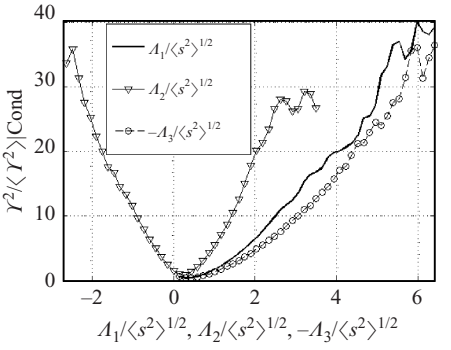

FIGURE 15. Conditional averages of the normalized square of the tilting vector, Υ^2, on the eigenvalues of the rate-of-strain tensor, Λ_k.

The PDFs of some quantities mentioned above are shown in figure 14. For example, the PDFs of eigen-contributions to $(W^{G_s})^2$, corresponding to pure stretching and compressing, are practically the same and contribute equally (because the eigenvalues enter here as Λ_k^2).

It is impossible to separate the eigen-contributions to the square of the tilting vector, Υ_i, since they enter in products. Indeed,

$$\Upsilon^2 = \Lambda_k^2\cos^2(\boldsymbol{G}, \boldsymbol{\lambda}_k) - [\Lambda_k\cos^2(\boldsymbol{G}, \boldsymbol{\lambda}_k)]^2 + (1/4)G^{-2}\overbrace{[G^2\omega^2 - (\boldsymbol{G}\cdot\boldsymbol{\omega})^2]}^{(\boldsymbol{G}\times\boldsymbol{\omega})^2}$$
$$+ G^{-1}[\boldsymbol{G}\times\boldsymbol{\omega}]\cdot\overbrace{[\Lambda_\alpha\cos(\boldsymbol{G}, \boldsymbol{\lambda}_\alpha)\mathbf{i}_\alpha]}^{G_ks_{\alpha k}} \quad \text{(no summation over } \alpha\text{)}. \qquad (4.2)$$

Therefore we show in figure 15 only conditional averages of Υ^2 on Λ_k ($k = 1, 2, 3$). The summary of the eigen-contributions is presented in table 3.

An additional view on the relations between $G_iG_js_{ij}$, $G_iG_js_{ij}/G^2$, Υ^2 and Λ_k ($k = 1, 2, 3$) is given by the corresponding joint PDFs (figures 16–18).

5. Geometrical statistics

By the term geometrical statistics we denote alignments between a variety of vectors.

Value	α	0.8 (m)	1.2 (m)	2.0 (m)	3.0 (m)	4.5 (m)	7.0 (m)	10.0 (m)
	1	−0.71	−0.64	−0.76	−0.67	−0.84	−0.69	−1.17
$-\langle G^2\Lambda_\alpha\cos^2(\boldsymbol{G},\boldsymbol{\lambda}_\alpha)\rangle$	2	0.11	−0.05	−0.06	−0.07	−0.08	−0.09	−0.12
	3	1.60	1.69	1.81	1.74	1.92	2.05	2.29
	1	0.09	0.26	0.30	0.23	0.25	0.26	0.27
$\langle G^2\Lambda_\alpha^2\cos^2(\boldsymbol{G},\boldsymbol{\lambda}_\alpha)\rangle$	2	0.14	0.03	0.03	0.02	0.03	0.02	0.03
	3	0.77	0.72	0.67	0.75	0.73	0.72	0.70
	1	−4.28	−2.11	−2.55	−2.49	−3.69	−4.51	−5.45
$-\langle\Lambda_\alpha\cos^2(\boldsymbol{G},\boldsymbol{\lambda}_\alpha)\rangle$	2	−0.40	−0.21	−0.23	−0.29	−0.41	−0.49	−0.59
	3	5.69	3.33	3.78	3.78	5.09	6.00	7.05
	1	0.32	0.35	0.41	0.34	0.36	0.37	0.37
$\langle\Lambda_\alpha^2\cos^2(\boldsymbol{G},\boldsymbol{\lambda}_\alpha)\rangle$	2	0.06	0.04	0.04	0.04	0.04	0.04	0.04
	3	0.61	0.61	0.54	0.63	0.60	0.60	0.59
	1	0.53	0.52	0.51	0.49	0.47	0.51	0.47
$\langle\Lambda_\alpha\rangle/\langle s^2\rangle^{1/2}$	2	0.09	0.10	0.09	0.07	0.06	0.09	0.06
	3	−0.62	−0.61	−0.60	−0.56	−0.53	−0.60	−0.53
	1	0.40	0.39	0.40	0.40	0.41	0.40	0.41
$\langle\Lambda_\alpha^2\rangle/\langle s^2\rangle$	2	0.04	0.04	0.04	0.05	0.05	0.04	0.06
	3	0.56	0.57	0.56	0.55	0.55	0.56	0.55
	1	0.48	0.53	0.54	0.52	0.76	0.46	0.60
$\langle\Lambda_\alpha^3\rangle/\langle s^2\rangle^{3/2}$	2	0.01	0.02	0.02	0.02	0.01	0.02	0.02
	3	−0.73	−0.82	−0.83	−0.86	−1.19	−0.80	−1.04

TABLE 3. Contribution of terms associated with the eigenvalues, Λ_α, of s_{ij} to the production of temperature fluctuations, $-G_iG_js_{ij} = -G^2\Lambda_k\cos^2(\boldsymbol{G},\boldsymbol{\lambda}_k)$, and its rate, $-G_iG_js_{ij}/G^2 = -\Lambda_k\cos^2(\boldsymbol{G},\boldsymbol{\lambda}_k)$, and square of the stretching vector, $(W^{G_s})^2 = G^2\Lambda_k^2\cos^2(\boldsymbol{G},\boldsymbol{\lambda}_k)$, and its rate, $(W^{G_s})^2/G^2 = \Lambda_k^2\cos^2(\boldsymbol{G},\boldsymbol{\lambda}_k)$, at various heights from the field experiment. The last rows show the means, the mean squares and the mean cubes of the eigenvalues of the rate-of-strain tensor, Λ_α; $s^2 = s_{ij}s_{ij} = \Lambda_1^2 + \Lambda_2^2 + \Lambda_3^2$; $s_{ij}s_{jk}s_{ki} = \Lambda_1^3 + \Lambda_2^3 + \Lambda_3^3$.

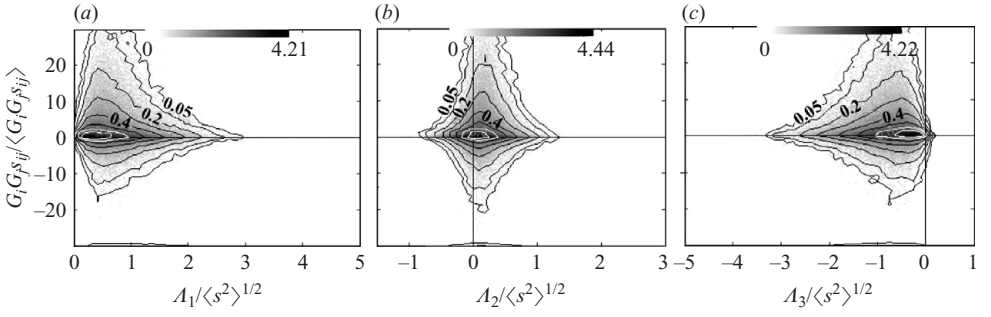

FIGURE 16. Joint PDFs of the normalized production of temperature fluctuations, $-G_iG_js_{ij} = -G^2\Lambda_k\cos^2(\boldsymbol{G},\boldsymbol{\lambda}_k)$, with the eigenvalues of the rate of strain tensor, Λ_k. (*a*) $k=1$, correlation coefficient = 0.073; (*b*) $k=2$, 0.080; (*c*) $k=3$, −0.141.

Among the main known features are the alignments of the temperature gradient, $\boldsymbol{G}$, and the eigenframe, $\boldsymbol{\lambda}_k$, of the rate-of-strain tensor, s_{ij}. These are shown in figure 19 and are qualitatively the same as in the DNS results at $Re_\lambda \sim 100$ in a cubic domain, mentioned above, the experimental results at $Re_\lambda \sim 800$ in a jet flow and those reported in experiments by Su & Dahm (1996) and in DNS by Flohr (1999) and Tsinober & Galanti (2001). The alignments of the temperature gradient, $\boldsymbol{G}$, and the eigenframe, $\boldsymbol{\lambda}_k$, of the rate-of-strain tensor, s_{ij}, become more pronounced

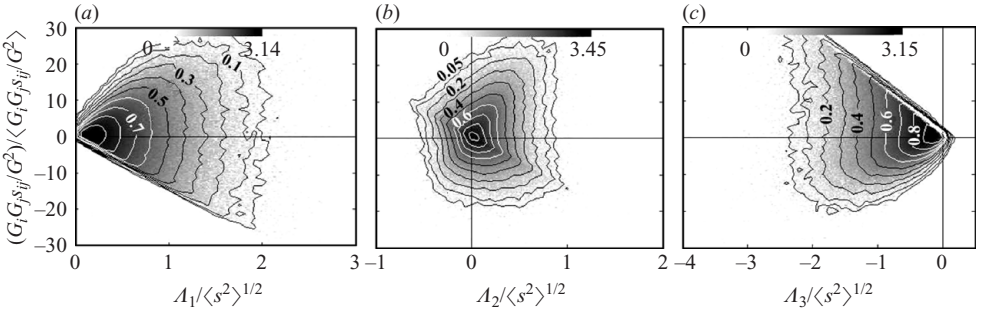

FIGURE 17. Joint PDFs of the normalized rate of production of temperature fluctuations, $-G_iG_js_{ij}/G^2 = -\Lambda_k\cos^2(\boldsymbol{G},\boldsymbol{\lambda}_k)$, with the eigenvalues of the rate of strain tensor, Λ_k. (*a*) $k=1$, correlation coefficient = 0.086; (*b*) $k=2$, 0.088; (*c*) $k=3$, −0.196.

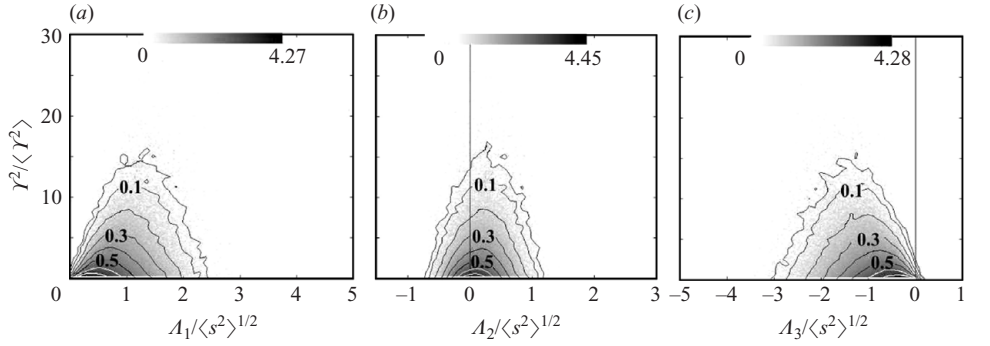

FIGURE 18. Joint PDFs of the normalized squared square of the tilting vector, Υ^2, with the eigenvalues of the rate-of-strain tensor, Λ_k. (*a*) $k=1$, correlation coefficient = 0.511; (*b*) $k=2$, 0.191; (*c*) $k=3$, −0.501.

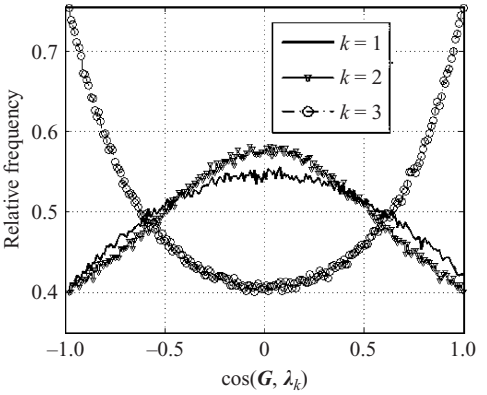

FIGURE 19. PDFs of the cosine of the angle between the temperature gradient vector, $\boldsymbol{G}$, and the eigenvectors, $\boldsymbol{\lambda}_k$, of the rate-of-strain tensor, s_{ij}.

at larger strains and magnitude of the temperature gradient, G, and weaker at larger enstrophy, ω^2 (figure 20).

A related kind of alignment of special interest is the alignment between the temperature gradient, G_i, and the stretching vector, $W_i^G \equiv -G_k(\partial u_k/\partial x_i)$, since their

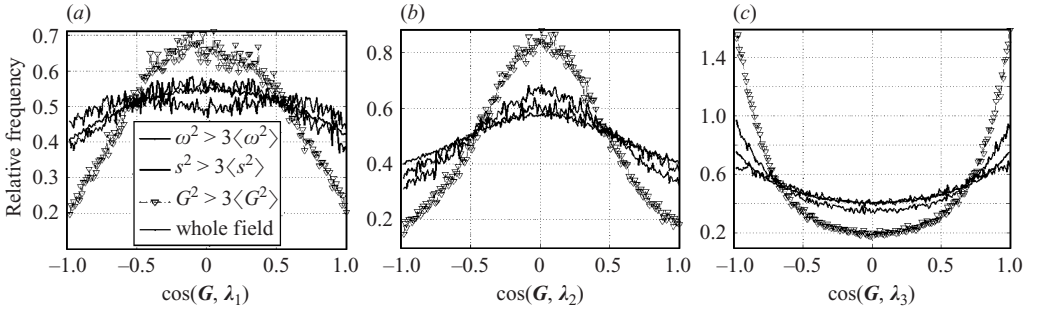

FIGURE 20. PDFs of the cosine of the angle between the temperature gradient vector, $\boldsymbol{G}$, and the eigenvectors, $\boldsymbol{\lambda}_k$, of the rate-of-strain tensor, s_{ij}. (*a*) $k=1$, (*b*) $k=2$, (*c*) $k=3$.

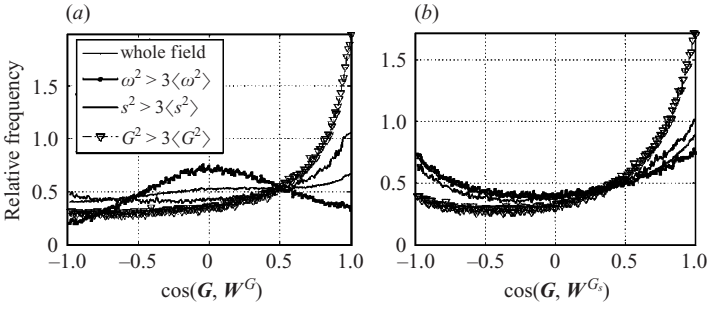

FIGURE 21. PDFs of the cosine of the angle between the temperature gradient vector, $\boldsymbol{G}$, and (*a*) the stretching vector, W_i^G, and (*b*) its component, $W_i^{G_s}$.

scalar product, $G_i W_i^G \equiv -G_i G_k(\partial u_k/\partial x_i) \equiv -G_i G_k s_{ik}$, is just the production term in (1.2). Therefore, it is natural to expect that the PDF of $\cos(\boldsymbol{G}, \boldsymbol{W}^G)$ should be positively skewed, as observed in figure 21(*a*). A similar behaviour is observed for the alignment between the temperature gradient, G_i, and the stretching vector, $W_i^{G_s} \equiv -G_k s_{ik}$, (figure 21*b*). Both exhibit stronger alignment for larger strains and magnitudes of the temperature gradient, G, and weaker alignment for larger enstrophy, ω^2.

We recall that

$$W_i^G \equiv -G_k \frac{\partial u_k}{\partial x_i} \equiv -G_k s_{ik} - \tfrac{1}{2}\varepsilon_{ijk} G_j \omega_k, \quad W_i^{G_s} \equiv -G_j s_{ij}, \quad W_i^{G_\omega} \equiv -\tfrac{1}{2}\varepsilon_{ijk}\omega_j G_k.$$

The vector $W_i^{G_s}$ is responsible for the production of G^2, whereas $W_i^{G_\omega}$ (which is normal to $\boldsymbol{G}$) rotates/tilts the vector $\boldsymbol{G}$, and $\cos(\boldsymbol{G}, \boldsymbol{W}^{G_\omega}) \equiv 0$ because $\boldsymbol{G} \perp \boldsymbol{W}^{G_\omega}$. Therefore, in order to characterize the effects of tilting of $\boldsymbol{G}$ it is useful to look at the quantity responsible for the change of its direction, i.e. the change of the direction of the unit vector, $\widehat{G}_i = G_i/G$. This is the inviscid tilting vector, $\Upsilon_i = -\widehat{G}_k(\partial u_k/\partial x_i) + \widehat{G}_i \widehat{G}_j \widehat{G}_k s_{jk}$, which enters the equation (1.3) governing the evolution of the unit vector, $\widehat{G}_i$. Typical results on the alignments of the tilting vector, $\boldsymbol{\Upsilon}$, and the eigenframe, $\boldsymbol{\lambda}_k$, of the rate-of-strain tensor, s_{ij}, are shown in figure 22. The first thing to note is that both pure stretching ($k=1$) and pure compression ($k=3$) result in identical alignment between $\boldsymbol{\Upsilon}$ and the corresponding eigen-directions, $\boldsymbol{\lambda}_1$ and $\boldsymbol{\lambda}_3$. The second feature is that the $\boldsymbol{\Upsilon}$, $\boldsymbol{\lambda}_k$ alignments are weakly sensitive to the magnitude of strain and vorticity, but change considerably with the magnitude of the temperature gradient, G.

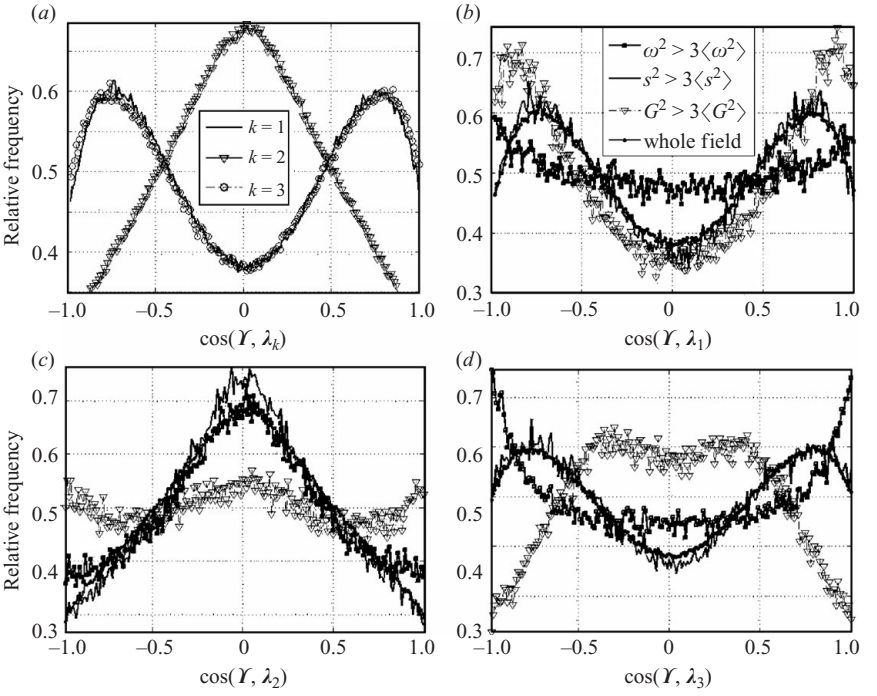

FIGURE 22. PDFs of the cosine of the angle between the inviscid tilting vector, $\boldsymbol{\Upsilon}$, and the eigenvectors, $\boldsymbol{\lambda}_k$, of the rate-of-strain tensor, s_{ij}. (*a*) $k=1-3$ for the whole field; (*b–c*) conditioned on the high values of ω^2, s^2 and G^2: (*b*) $k=1$, (*c*) $k=2$, (*d*) $k=3$.

5.1. *Production versus its surrogate*

As mentioned, it is customary to represent the production of the temperature gradient, $-G_iG_ks_{ik}$, by its surrogate, $-(\partial u_1/\partial x_1)(\partial\theta/\partial x_1)^2$. For isotropic flow

$$\langle(\partial u_1/\partial x_1)(\partial\theta/\partial x_1)^2\rangle = (2/15)\langle G_iG_ks_{ik}\rangle.$$

Moreover, it appears from our measurements that the PDFs of $(\partial u_1/\partial x_1)(\partial\theta/\partial x_1)^2$ and $(2/15)G_iG_ks_{ik}$ are very similar as well (figure 23), indicating the tendency to isotropy in small scales by this particular criterion. However, this still does not mean that the true production, $G_iG_ks_{ik}$, is fully represented by its surrogate, $(\partial u_1/\partial x_1)(\partial\theta/\partial x_1)^2$. Indeed, as seen from their joint PDF, this is not the case as it would be if the shape of this joint PDF were close to the bisector.

5.2. *Vorticity versus G*

The differently normalized enstrophy production, $\omega_i\omega_js_{ij}/(\omega^2 s)$, and production of temperature gradient, $-G_iG_js_{ij}/(G^2 s)$, shown in figure 24, reveal two aspects. The first is that, again, the behaviour is qualitatively the same for a Taylor microscale Reynolds number of the order of 10^2 and 10^4. The second aspect is that the production of enstrophy is considerably different from that of temperature gradient.

Another reason for comparison of $\boldsymbol{\omega}$ and $\boldsymbol{G}$ is that for the inviscid and non-diffusive flows the scalar product, $\boldsymbol{\omega}\cdot\boldsymbol{G}$, is a Lagrangian pointwise invariant, i.e. it is conserved along fluid particle trajectories. The PDF of $\cos(\boldsymbol{\omega}, \boldsymbol{G})$ is shown in figure 25.

An additional aspect of comparison is shown in figure 26 with the alignments of the vorticity tilting vector, $\boldsymbol{\Upsilon}^{\omega}$, and the temperature gradient tilting vector, $\boldsymbol{\Upsilon}^{G}$, with

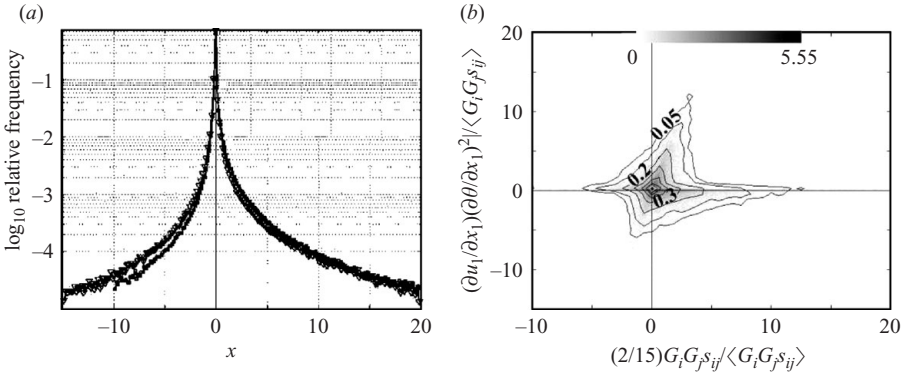

FIGURE 23. (*a*) PDFs of the true production of the temperature gradient, $-G_iG_ks_{ik}$, and its surrogate, $-(\partial u_1/\partial x_1)(\partial\theta/\partial x_1)^2$, and (*b*) their joint PDF. (*a*) ●, $x=(2/15)\ G_iG_js_{ij}/\langle G_iG_js_{ij}\rangle$; ∇, $x=(\partial u_1/\partial x_1)\ (\partial\theta/\partial x_1)^2/\langle G_iG_js_{ij}\rangle$. (*b*) Correlation coefficient = 0.112.

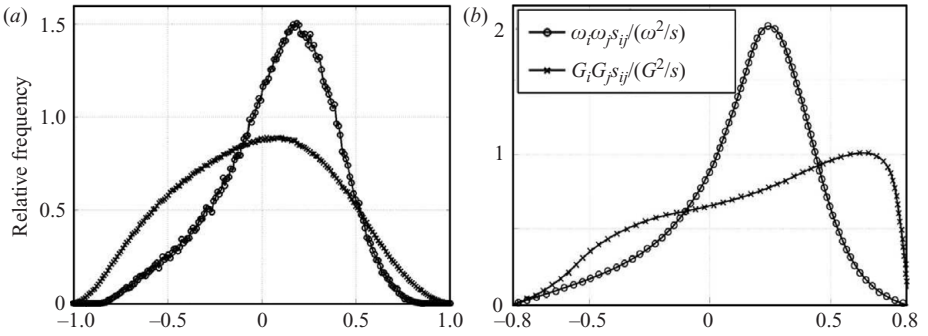

FIGURE 24. PDFs of normalized enstrophy production, $\omega_i\omega_js_{ij}/(\omega^2s)$, and production of temperature gradient, $-G_iG_js_{ij}/(G^2s)$. (*a*) Field experiment and (*b*) direct numerical simulation of Navier–Stokes equations (Brethouwer *et al.* 2003).

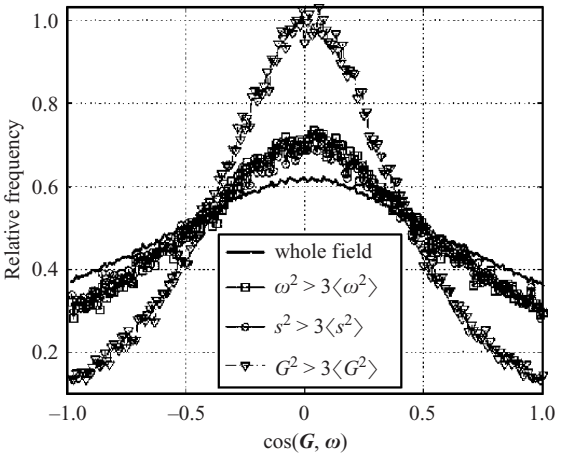

FIGURE 25. PDFs of the cosine of the angle between the temperature gradient vector, $\boldsymbol{G}$, and the vorticity vector, $\boldsymbol{\omega}$, for the whole field and conditioned on the high values of ω^2, s^2 and G^2.

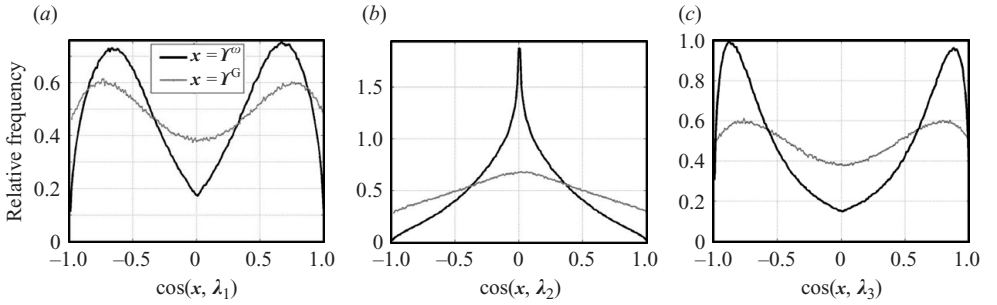

FIGURE 26. PDFs of the cosine of the angle between the vorticity tilting vector, $\boldsymbol{\Upsilon}^{\boldsymbol{\omega}}$, and the temperature gradient tilting vector, $\boldsymbol{\Upsilon}^{\boldsymbol{G}}$, with eigen-frame of the rate-of-strain tensor, s_{ij}.

eigen-frame of the rate-of-strain tensor, s_{ij}. Only a qualitative resemblance can be noted. Both $\boldsymbol{\Upsilon}^{\boldsymbol{\omega}}$ and $\boldsymbol{\Upsilon}^{\boldsymbol{G}}$ tend to be orthogonal to the intermediate eigenvector, $\boldsymbol{\lambda}_2$, and to be aligned with the other two eigenvectors.

6. Concluding remarks

The main technical achievement is that the possibility of obtaining experimentally joint statistics of velocity gradients and temperature gradients is demonstrated and a number of related results are obtained. Another aspect is the implementation of a multi-hot–cold-wire technique which allowed us to perform measurements of the streamwise derivatives without invoking the Taylor hypothesis.

The results obtained in this work are in full conformity with those obtained in our previous field experiments (Kholmyansky & Tsinober 2000; Kholmyansky *et al.* 2000, 2001*a*, *b*; Galanti *et al.* 2003). Being the first repetition of an experiment, in which explicit information is obtained on the field of velocity derivatives, it gives us confidence in both experiments. Therefore, the results reported here confirm the main conclusions made before. Namely, results from high Re_λ field experiments are similar to those obtained in experiments in laboratory turbulent grid flow and in DNS of Navier–Stokes equations in a cubic domain with periodic boundary conditions, both at $Re_\lambda \sim 10^2$. An important aspect is that this similarity is not only qualitative, but to a large extent quantitative. The main difference between the two is in the 'length' of the inertial range. This means that the basic physics of turbulent flow at high Reynolds number, $Re_\lambda \sim 10^4$, at least qualitatively, is the same as at moderate Reynolds numbers, $Re_\lambda \sim 10^2$. This is true of such basic processes as enstrophy and strain production, geometrical statistics, the role of concentrated vorticity and strain, reduction of nonlinearity and non-local effects, fluid particle accelerations and quantities related to temperature and its gradient.

Among the specific results of importance is the essential difference in the behaviour of the production of temperature gradients in regions dominated by vorticity and strain. Namely, the production of temperature gradients is much more intensive in regions dominated by strain, whereas production of temperature gradients is practically independent of the magnitude of vorticity. In contrast, vorticity and strain are contributing equally to the tilting of the vector of temperature gradients. The production of temperature gradients is mainly due to the fluctuative strain, the terms associated with mean fields are unimportant.

It was checked directly (by looking at corresponding eigen-contributions and alignments) that the production of the temperature gradients is due to predominant

compressing of fluid elements rather than stretching, which is true of other processes in turbulent flows, e.g. turbulent energy production in shear flows.

Though the production of the temperature gradient and its surrogate possess similar univariate PDFs (which indicates the tendency to isotropy in small scales by this particular criterion), their joint PDF is not close to a bisector. This means that the true production of the temperature gradient is far from being fully represented by its surrogate.

Our results were obtained with cold wires 2.5 μm thick. Therefore, they were under-resolved in the smallest scales. In order to obtain adequate resolution in the smallest scales, the cold wires should be about 1 μm thick along with improvements in the system such as (i) the probe construction requiring further miniaturization of its individual arrays as well as of the whole probe, and (ii) further improvement of the calibration system along with the use of higher-quality electronic equipment. This will allow us to address a number of issues concerning the small scales of the temperature field not touched on in this study.

This work was supported in part by the Israel Science Foundation (ISF), founded by the Israel Academy of Sciences and Humanities, Research grant 34/02; the United States – Israel Binational Science Foundation (BSF), No. 2002264. The field experiment in Switzerland was supported by the Vice President for Research of ETH, Zürich.

The authors appreciate the assistance provided by Dr K. W. Hoyer and Mr T. Blunschi from ETH.

REFERENCES

Ashurst, W. T., Kerstein, A. R., Kerr, R. M. & Gibson, C. H. 1987 Alignment of vorticity and scalar gradient with strain rate in simulated Navier–Stokes turbulence. *Phys. Fluids* **30**, 2343–2353.

Batchelor, G. K. & Townsend, A. A. 1956 Turbulent diffusion. In *Surveys in Mechanics* (ed. G. K. Batchelor & R. M. Davies), pp. 352–399. Cambridge University Press.

Brethouwer, G., Hunt, J. C. R. & Nieuwstadt, F. T. M. 2003 Micro-structure and Lagrangian statistics of the scalar field with a mean gradient in isotropic turbulence. *J. Fluid Mech.* **474**, 193–225.

Corrsin, S. 1953 Remarks on turbulent heat transfer. An account of some features of the phenomenon in fully turbulent region. In *Proceedings of the First Iowa Symposium on Thermodynamics*, pp. 5–30. State University of Iowa, Iowa City.

Dimotakis, P. E. 2001 Recent developments in turbulent mixing. In *Mechanics for New Millenium* (ed. H. Aref & J. W. Phillips), pp. 327–344. Kluwer.

Falkovich, G., Gawedzki, K. & Vergassola, M. 2001 Particles and fields in fluid turbulence. *Rev. Mod. Phys.* **73**, 913–975.

Flohr, P. 1999 Small-scale flow structure in turbulence: fundamentals and numerical models. PhD thesis, Wolfson College, University of Cambridge.

Galanti, B., Gulitsky, G., Kholmyansky, M., Tsinober, A. & Yorish, S. 2003 Velocity derivatives in turbulent flow in an atmospheric boundary layer without Taylor hypothesis. In *Turbulence and Shear Flow Phenomena* (ed. N. Kasagi, J. K. Eaton, R. Friedrich, J. A. C. Humphrey, M. A. Leschziner & T. Miyauchi), vol. 2, pp. 745–750.

Gibson, C. H., Ashurst, W. T. & Kerstein, A. R. 1988 Mixing of strongly diffusive passive scalars like temperature by turbulence. *J. Fluid Mech.* **194**, 261–293.

Girimaji, S. S. & Pope, S. B. 1990 Material-element deformation in isotropic turbulence. *J. Fluid Mech.* **220**, 427–458.

Gonzalez, M. 2002 Effect of vorticity on second- and third-order statistics of passive scalar gradients. *Phys. Rev.* E **65**, 056307/1–8.

Gonzalez, M. & Paranthoën, P. 2004 On the role of vorticity in the microstructure of a passive scalar field. *Phys. Fluids* **16**, 219–221.

Guala, M., Lüthi, B., Liberson, A., Tsinober, A. & Kinzelbach, W. 2005 On the evolution of material lines and vorticity in homogeneous turbulence. *J. Fluid Mech.* **533**, 339–359.

Gulitski, G., Kholmyansky, M., Kinzelbach, W., Lüthi, B., Tsinober, A. & Yorish, S. 2007 Velocity and temperature derivatives in high-Reynolds-number turbulent flows in the atmospheric surface layer. Part 1. Facilities, methods and some general results. *J. Fluid Mech.* **589**, 57–81.

Kholmyansky, M. & Tsinober, A. 2000 On the origins of intermittency in real turbulent flows. In *Proceedings of the Symposium on Intermittency in turbulent flows and other dynamical systems held at Isaac Newton Institute, Cambridge, June 21–24, 1999* (ed. J. C. Vassilicos). Isaac Newton Institute for Mathematical Sciences, Preprint NI99017-TRB. Cambridge University Press.

Kholmyansky, M., Tsinober, A. & Yorish, S. 2000 Geometrical statistics in the atmospheric turbulent flow at $Re_\lambda = 10^4$. *Adv. Turbulence* **8**, 895–898.

Kholmyansky, M., Tsinober, A. & Yorish, S. 2001*a* Velocity derivatives in the atmospheric surface layer at $Re_\lambda = 10^4$. *Phys. Fluids* **13**, 311–314.

Kholmyansky, M., Tsinober, A. & Yorish, S. 2001*b* Velocity derivatives in the atmospheric surface layer at $Re_\lambda = 10^4$. Further results. In *Proceedings of the Second International Symposium on Turbulence and Shear Flow Phenomena, Stockholm, June, 27–29, 2001* (ed. E. Lindborg, A. Johansson, J. Eaton, J. Humphrey, N. Kasagi, M. Leschziner & M. Sommerfeld), vol. 1, pp. 109–113.

Majda, A. J. & Kramer, P. R. 1999 Simplified models for turbulent diffusion: theory, numerical modelling, and physical phenomena. *Phys. Rep.* **314**, 237–574.

Pumir, A. 1994 A numerical study of the mixing of a passive scalar in three dimensions in the presence of a mean gradient. *Phys. Fluids* **6**, 2118–2132.

Ruetsch, G. R. & Maxey, M. R. 1991 Small-scale features of vorticity and passive scalar fields in homogeneous turbulence. *Phys. Fluids* A **3**, 1587–1597.

Ruetsch, G. R. & Maxey, M. R. 1992 The evolution of small-scale structures in homogeneous isotropic turbulence. *Phys. Fluids* A **4**, 2747–2760.

Sawford, B. 2001 Turbulent relative dispersion. *Annu. Rev. Fluid Mech.* **33**, 289–317.

Shen, X. & Warhaft, Z. 2000 The anisotropy of the small scale structure in high Reynolds number ($R_\lambda \sim 1000$) turbulent shear flow. *Phys. Fluids* **12**, 2976–2989.

Shraiman, B. I. & Siggia, E. D. 2000 Scalar turbulence. *Nature* **405**, 639–646.

Sreenivasan, K. R. & Antonia, R. 1997 The phenomenology of small-scale turbulence. *Annu. Rev. Fluid Mech.* **29**, 435–472.

Su, L. K. & Dahm, W. J. A. 1996 Scalar imaging velocimetry measurements of the velocity gradient tensor field in turbulent flows. ii. Experimental results. *Phys. Fluids* **8**, 1883–1906.

Tsinober, A. 2001 *An Informal Introduction to Turbulence*. Kluwer.

Tsinober, A. & Galanti, B. 2001 Numerical experiments on geometrical statistics of passive objects in turbulent flows. Presentation at EUROMECH Workshop 428 *Transport by Coherent Structures in Environmental and Geophysical Flows*, Torino, 26–29 September 2001.

Tsinober, A. & Galanti, B. 2003 Exploratory numerical experiments on the differences between genuine and 'passive' turbulence. *Phys. Fluids* **15**, 3514–3531.

Vedula, P., Yeung, P. K. & Fox, R. O. 2001 Dynamics of scalar dissipation in isotropic turbulence: a numerical and modelling study. *J. Fluid Mech.* **433**, 29–60.

Villermaux, E. 2001 Mixing: kinetics and geometry. In *Mechanics for New Millenium* (ed. H. Aref & J. W. Phillips), pp. 165–180. Kluwer.

Warhaft, Z. 2000 Passive scalars in turbulent flows. *Annu. Rev. Fluid Mech.* **32**, 203–240.